Volume Reconstruction of Large Tissue Specimens From Serial Physical Sections Using Confocal Microscopy and Correction of Cutting Deformations by Elastic Registration

MARTIN ČAPEK,[1,2]* PETR BRŮŽA,[1,2] JIŘÍ JANÁČEK,[1] PETR KAREN,[1]
LUCIE KUBÍNOVÁ,[1] AND RADOMÍRA VAGNEROVÁ[3]
[1]*Department of Biomathematics, Institute of Physiology, Academy of Sciences of the Czech Republic, v.v.i., Vídeňská 1083, 142 20 Prague 4 - Krč, Czech Republic*
[2]*Joint Department of Biomedical Engineering of the Faculty of Biomedical Engineering and the 1st Medical Faculty, Czech Technical University in Prague, 272 01 Kladno 2, Czech Republic*
[3]*Institute of Histology and Embryology, First Faculty of Medicine, Charles University in Prague, 128 00 Prague 2, Czech Republic*

KEY WORDS 3D reconstruction; elastic registration; 3D visualization; confocal microscopy

ABSTRACT A set of methods leading to volume reconstruction of biological specimens larger than the field of view of a confocal laser scanning microscope (CLSM) is presented. Large tissue specimens are cut into thin physical slices and volume data sets are captured from all studied physical slices by CLSM. Overlapping spatial tiles of the same physical slice are stitched in horizontal direction. Image volumes of successive physical slices are linked in axial direction by applying an elastic registration algorithm to compensate for deformations because of cutting the specimen. We present a method enabling us to keep true object morphology using a priori information about the shape and size of the specimen, available from images of the cutting planes captured by a USB light microscope immediately before cutting the specimen by a microtome. The errors introduced by elastic registration are evaluated using a stereological point counting method and the Procrustes distance. Finally, the images are enhanced to compensate for the effect of the light attenuation with depth and visualized by a hardware accelerated volume rendering. Algorithmic steps of the reconstruction, namely elastic registration, object morphology preservation, image enhancement, and volume visualization, are implemented in a new *Rapid3D* software package. Because confocal microscopes get more and more frequently used in scientific laboratories, the described volume reconstruction may become an easy-to-apply tool to study large biological objects, tissues, and organs in histology, embryology, evolution biology, and developmental biology. In this work, we demonstrate the reconstruction using a postcranial part of a 17-day-old laboratory Wistar rat embryo. *Microsc. Res. Tech. 72:110–119, 2009.*

INTRODUCTION

Three-dimensional (3D) or volume reconstruction of biological tissue specimens using a confocal laser scanning microscope (CLSM) can show biologists 3D arrangement of various organs, tissue structures, and cells. For this purpose, CLSM enables us to acquire a stack (series) of images of perfectly registered optical sections, i.e., a 3D image, representing the investigated biological specimen via optical sectioning and scanning of 2D confocal planes (Pawley, 2006).

In this article, we address the volume reconstruction of biological specimens larger than one stack of images that can be captured by CLSM, both in lateral and axial directions. When one-photon excitation is applied, the axial field of view of CLSM is restricted to not more than 200 μm (Diaspro et al., 2006). Two-photon excitation allows us to focus through theoretically up to several hundred micrometers (Diaspro, 2002). In practice, lower depths are usually achieved either because of the attenuation of fluorescence signal with depth, or the restricted working distance of high-resolution objectives.

If the size of a specimen to be investigated exceeds the lateral field of view of CLSM, then a number of overlapping fields of view covering the whole specimen have to be captured, and the image representation of the whole specimen is obtained by a suitable software tool via image mosaicking (e.g., Čapek and Krekule, 1999; Karen et al., 2003; Lee and Bajcsy, 2005). If, furthermore, the thickness of the specimen exceeds the maximal depth that CLSM can focus through, the specimen is cut into serial physical slices of adequate thickness. The image representation of the whole specimen is then obtained by applying methods of volume reconstruction.

A number of authors dealt with 3D volume reconstruction from microscopic data. Volume reconstruction

*Correspondence to: Martin Čapek, Institute of Physiology, Academy of Sciences of the Czech Republic, v.v.i., Vídeňská 1083, 142 00 Prague 4 - Krč, Czech Republic. E-mail: capek@biomed.cas.cz

Received 6 June 2008; accepted in revised form 19 September 2008

Contract grant sponsor: Ministry of Education, Youth, and Sports, Czech Republic; Contract grant numbers: MSM6840770012, MSM0021610807, and LC06063; Contract grant sponsor: Academy of Sciences, Czech Republic; Contract grant numbers: A100110502, A500200510, and AV0Z 50110509; Contract grant sponsor: Czech Science Foundation, Czech Republic; Contract grant number: 102/08/0691.

DOI 10.1002/jemt.20652

Published online 10 November 2008 in Wiley InterScience (www.interscience.wiley.com).

from one stack of optical sections captured by CLSM with emphasis on image enhancement and comparison of surface versus volume rendering visualizations were demonstrated by Liu et al. (1997). Some works described reconstruction from serial physical or histological sections acquired by an electron microscope, (Lee et al., 2005; Ovtscharoff et al., 2008), a transmission microscope (Cerri et al., 2004; Cornillie et al., 2008), and a fluorescence microscope (Duerstock, 2004; Kurien et al., 2005). Single images or photomicrographs per one physical section were used there, and the reconstruction was achieved by employing various free or commercial standard software packages available on the internet, e.g., *Reconstruct* software, http://synapses.clm.utexas.edu/tools/index.stm. A computer-assisted microscopic system for 3D reconstruction and analysis, introduced by Fernandez-Gonzales et al. (2002), rendered volumes also from single fluorescence images captured from serial physical sections. Papadimitriou et al. (2004) described a special way of preparation of physical sections using a truncated pyramidal specimen shape in order to achieve precise and reliable volume reconstruction. Accuracy of 3D reconstructions from serial histological sections was evaluated by Duerstock et al. (2003). Volume reconstructions from optical sections captured from single physical sections by CLSM were presented, e.g., by Jirkovská et al. (2002). This article also highlighted the advantages of volume reconstruction for investigation of topological properties and spatial arrangement of structures in thick tissues. Enhancement of confocal data sets for high-quality visualization and measurement of reconstructed volumes was reported by Difato et al. (2004).

Not too many articles described volume reconstruction from stacks of optical sections captured by CLSM from multiple physical slices. Mosaicking of overlapping stacks of optical sections captured from one physical slice and alignment of mosaicked 3D images of successive physical slices were presented by Karen et al. (2003) and Lee and Bajcsy (2005). In the former work, the authors used a semiautomatic approach based on user-inserted starting control points that facilitate the reconstruction process, whereas a semiautomatic segmentation of salient features present in images was employed in the latter work. The feature-based approach was further developed by Lee and Bajcsy (2007). A multistep approach to volume reconstruction including, in particular, the selection and segmentation of regions of interest, computation and matching of salient features (centroids, areas), transformation of 3D images, and enhancement of image intensities in the resulting 3D volumes was described by Bajcsy et al. (2006).

In this article, we present a complex approach to volume reconstruction of large biomedical tissue specimens. This work follows up our previous article (Karen et al., 2003), where we described reconstruction using only image translation and rotation. Our new, improved approach, see Figure 1., consists of embedding the specimen into a paraffine block and using this nondeparaffinized specimen for reconstruction (A); Cutting the specimen into physical slices while simultaneously recording pictures of the block's cutting plane by a USB light microscope to obtain a priori image information about the original size and shape of the specimen (B); Acquisition of data by a confocal microscope (C); Composition of a high-resolution image by using suitable registration techniques, incorporating images captured by the USB light microscope to recover original shape and size of the specimen (D, E); Image enhancement of optical sections in the resulting volume using algorithms developed in our group (F). The resulting volume is visualized by hardware-accelerated volume rendering.

The elastic registration part of the reconstruction, the recovery of shapes and sizes of objects during reconstruction using the light microscope images, image enhancement of optical sections, and volume visualization of reconstructed volumes are the main improvements over our previous work (Karen et al., 2003). These steps are integrated into our new *Rapid3D* software package.

The volume reconstruction described above represents a set of methods that can be easily applied in every laboratory having access to a confocal microscope, which becomes a more and more exploited tool in biology. The approach is universal and suitable for study of large biological objects, tissues, and organs, for example, in histology, embryology, and evolution biology. In this article, we demonstrate the methods on the 3D reconstruction of a postcranial part of a 17-day-old laboratory Wistar rat embryo.

MATERIALS AND METHODS

Specimen Preparation

A 17-day-old embryo of a rat was fixed for 24 h in fixative (10% formalin with 1% eosin). After dehydration, the embryo was embedded in paraffine. Then 30-μm-thick physical slices were cut by a rotary microtome HM 340 E (MICROM Laborgeräte, Walldorf, Germany). Using the nondeparaffinized slices for acquisition of confocal data increased stability and lowered deformations of the specimens that occur when slices are manipulated after cutting. The process of the specimen preparation was described in detail by Jirkovská et al. (2005), where we found that for paraffine-embedded physical slices the thickness of 30–40 μm was the most suitable for volume reconstruction. In thicker specimens, we encountered a strong decrease of image intensities with depth.

Acquisition of Light Microscope Images

The specimen embedded in the paraffine block was mounted on the microtome, which was equipped with a stationary knife holder and a forward-moving block holder. A USB light microscope Dino-Lite AM 413T was placed in front of the microtome, and its optical axis was aligned with the upper turning point of the block holder excursion. At this point, the block stopped at approximately the same position during the acquisition of the picture. A ring with eight UV LEDs was attached to the microscope objective. For our experiment magnification 45× was chosen. Color images (1280 × 1024 pixels) of the cutting planes of the paraffine block were captured before cutting the corresponding physical slices. In case of specimens embedded in paraffine, the USB light microscope provided us with images having less detailed structures than CLSM, however, these images contained main features of depicted objects—borders, shapes and sizes—necessary for subsequent image processing. Moreover, the USB

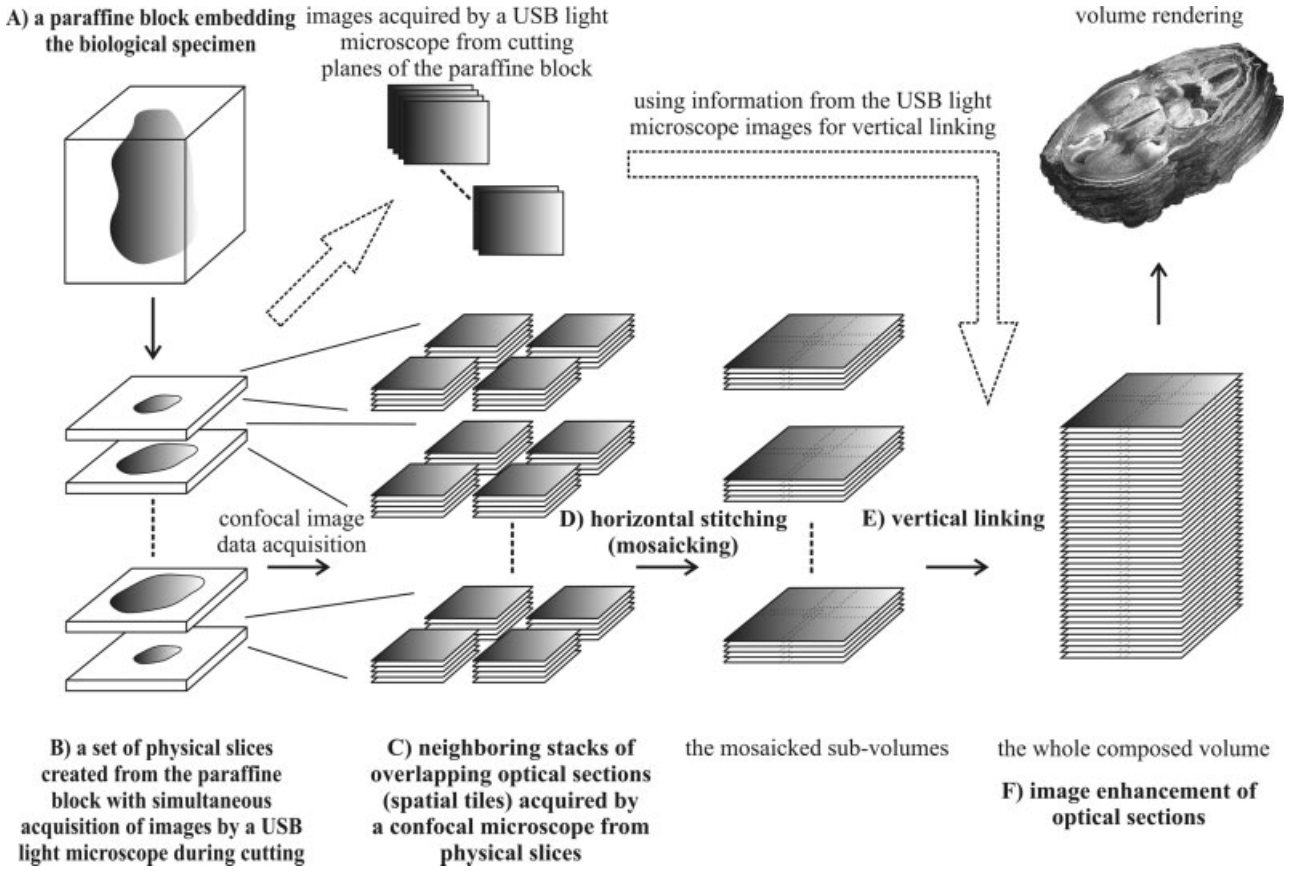

Fig. 1. An overview of 3D volume reconstruction of a thick biological tissue specimen using a confocal microscope.

light microscope was small, portable and easy to attach to the used microtome.

We captured one USB light microscope image per each microscopic slide carrying six to eight physical sections. Ten microscopic slides were used for the rat embryo example in this article, and thus 10 USB light microscope images and 64 physical slices entered the reconstruction procedure described below.

Acquisition of Confocal Images

Sixty four successive physical sections of the rat embryo were captured by a Leica SPE CLSM using a 5× HC PL FLUOTAR dry objective, NA = 0.15. Each physical section was split into six to eleven overlapping horizontal fields of view, and the corresponding stacks of optical sections were acquired using a manual microscopic stage. Excitation wavelength applied to the specimen was 488 nm and emission wavelengths ranged from 500 to 560 nm. The resulting stacks contained four optical sections scanned 9.7 μm apart in z-direction. Thus, 256 stacks of optical sections, each section consisting of 512 × 512 pixels, entered the following volume reconstruction steps.

Horizontal Stitching (mosaicking)

For proper image mosaicking, the problem of image registration had to be solved—for overview of image registration techniques see, for example, Zitová and Flusser (2003). In our case, mosaicking required to find parameters of geometrical transformation that stitch spatial tiles together, using information within their overlapping parts, see also Figure 2. One spatial tile was considered to be fixed whereas the second one was transformed (floating) to be stitched with the fixed tile.

Registration can be expressed by the formula

$$T' = \arg\min_T F(u(.), v(T(.))), \quad (1)$$

where T is geometrical transformation applied to a spatial tile to be transformed, T' is geometrical transformation which is searched for, F stands for a similarity measure evaluating the quality of registration (see below), $u(.)$ is the fixed spatial tile and $v(T(.))$ is the transformed (floating) spatial tile.

Because spatial tiles belonging to the same physical slice were obtained by moving the microscope stage, it was necessary to find their correct mutual translations. Registration procedure started by insertion of a pair of starting control points (landmarks) for finding the initial position of the spatial tiles, followed by the automatic refinement of the mutual position of tiles, using a suitable similarity measure, such as normalized correlation coefficient, sum of absolute valued differences, or mutual information. The similarity measure was optimized in the parametrical space of translations by *n-step search* (Tekalp, 1995). The optimization strategy

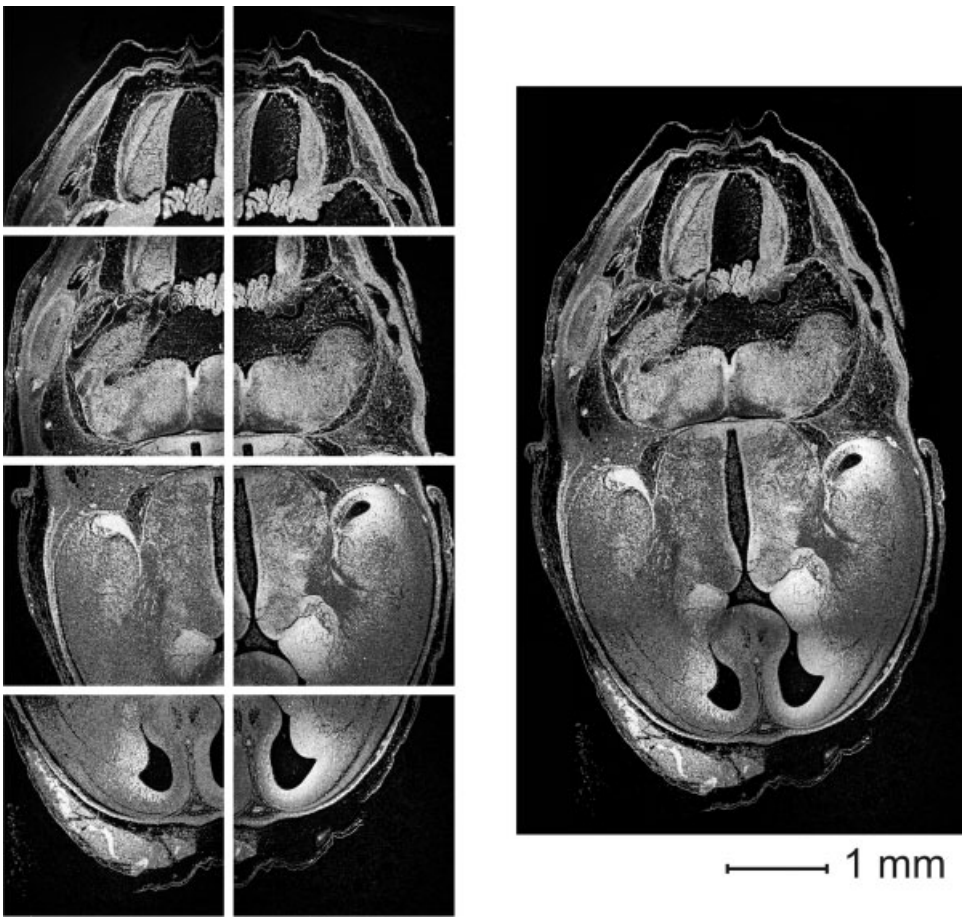

Fig. 2. Horizontal stitching (mosaicking) of eight overlapping fields of view of a physical slice of a rat embryo (left) into a resulting mosaicked image (right).

was based on decreasing searching steps to achieve a global optimum of a similarity measure between overlaps of neighboring spatial tiles. In the first level, *n-step search* searched an optimum of chosen similarity measure in a predefined parametric space using a big step of translation. After finding an optimum of the measure the search step was decreased, and the optimization continued only in the vicinity of the previous result to hit the optimum precisely. This procedure was repeated n times, with n being equal to three as a compromise between accuracy and speed. The algorithm was implemented in the *GlueMRC* software (Karen et al., 2003).

Vertical Linking While Incorporating Information From USB Light Microscope Images

The physical cutting of large specimens introduced spatial discrepancies between successive physical slices. These discrepancies were created mainly by the cutting tool and by deformations during preparation—partial mechanical damage of the specimen, off-cut resulting in the loss of some information between each pair of successive physical slices, shrinkage because of dehydration of slices, etc.

To perform the reconstruction, we needed to compensate for deformations, and register images of one physical slice with images of the next physical slice, see Figure 3. Because of the extent of above described deformations, it was difficult to apply pixel-based registration procedures only, because these usually end in local minima and, thus, give erroneous results. Therefore, we applied a registration algorithm initialized by user inserted landmarks, followed by refinement of the registration using a similarity measure.

A suitable algorithm for elastic registration was published by Sorzano et al. (2005). The algorithm was also implemented as a plug-in for open-source *ImageJ* software (http://rsbweb.nih.gov/ij/). We ported this algorithm using the original source code available at *ImageJ* web page from Java to C# language. We implemented it within *Rapid3D* software package for volume reconstruction and adapted it to the registration of stacks of optical sections, i.e., 3D images.

The resulting reconstructed volume was created by systematic composition and adding images of physical slices using elastic registration. The mutually deformed images were thus aligned; however, this brought about propagation of the deformations through the reconstructed volume. For example, if sections of a

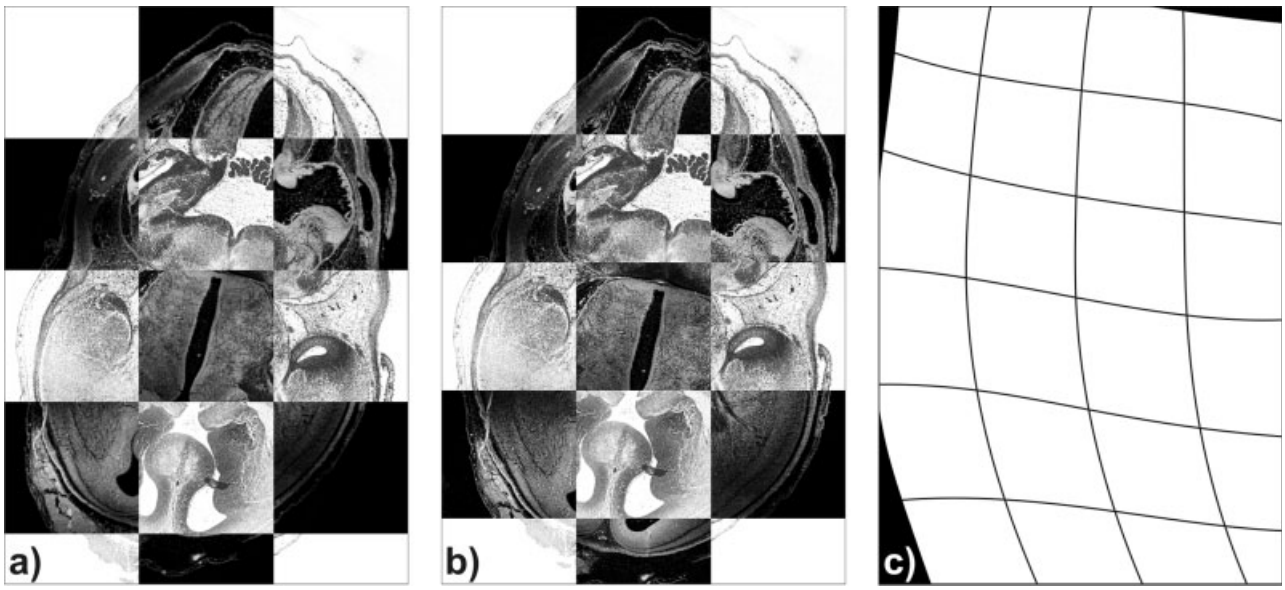

Fig. 3. Example of elastic registration of confocal images of successive physical slices: (**a**) chessboard-merged images distinguished by gray levels before registration (negative image–fixed, positive image–floating), (**b**) chessboard-merged images distinguished by gray levels after registration (negative image–fixed, positive image–floating), (**c**) applied elastic deformation mask—the black image had to be stretched especially in *x* direction to match the white one.

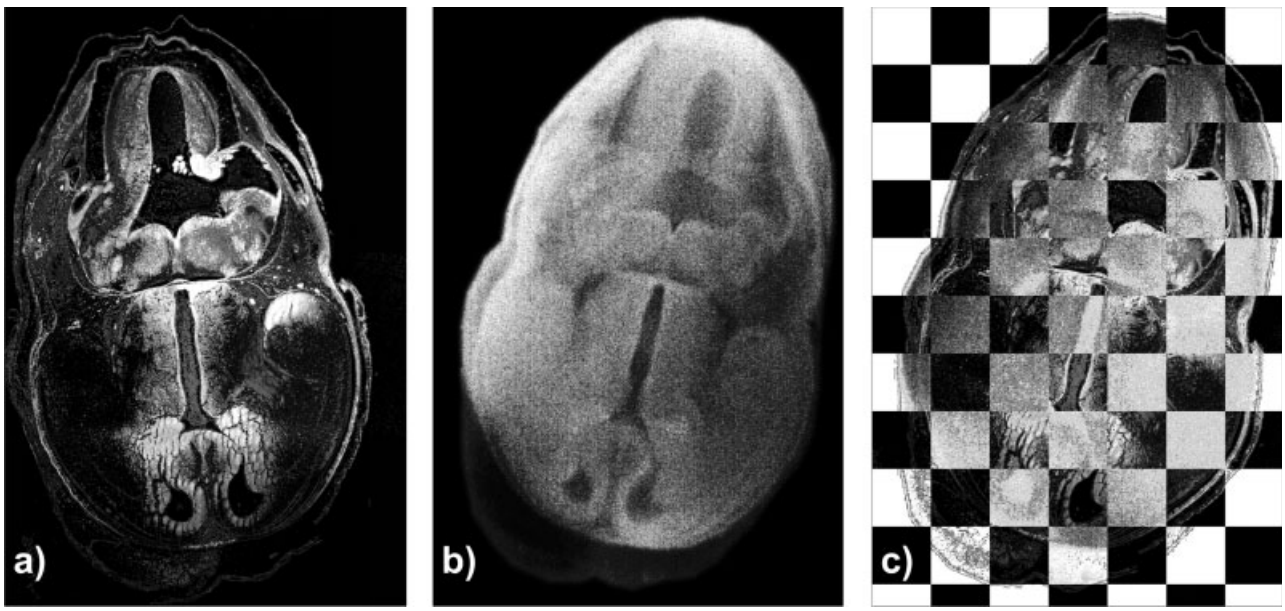

Fig. 4. Example of elastic registration of a confocal image (**a**) with a corresponding USB light microscope image (**b**). The image (**c**) Represents chessboard-merged images distinguished by gray levels after registration (negative image–fixed, positive image–floating).

"cone-like" object were reconstructed, by using elastic registration we would obtain a "cylinder-like" one, which was not desired.

We solved the problem of propagation of deformations through the reconstructed volume by recording the shape of investigated objects by a USB light microscope prior to cutting. The shape of objects was then restored after elastic registration using information in the captured pictures. We proposed the following two consecutive procedures for compensation of the undesirable deformation propagation.

In the first procedure, we registered and corrected subvolumes of physical slices carried by one microscopic slide by using one USB light microscope image.

The first procedure (Figs. 4 and 5):

Input data (for one iteration): A USB light microscope image and stacks of mosaicked confocal images (subvolumes) corresponding to physical slices

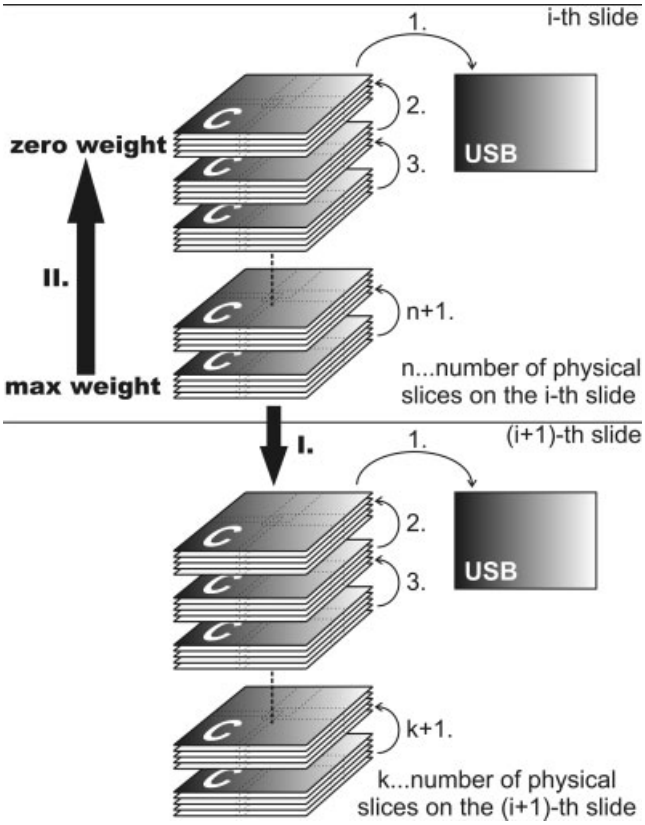

Fig. 5. Vertical linking incorporating information from USB light microscope images, see text. "C" means confocal mosaicked data; "USB" stands for USB light microscope images. Curved arrows denote alignments and they point in the direction from floating data sets to fixed data sets. "Weight" lowers the influence of elastic transformation on confocal images, see text.

lying on one microscopic slide. Distance calibration of images.

1. Landmark-based elastic registration of the confocal image (captured from the first physical slice on the microscopic slide) with the USB light microscope image (captured from the cutting plane of the first physical slice). The USB light microscope image was a reference picture (fixed), the confocal image was elastically transformed (floating), see Figure 4. Thus, the shape and size of the confocal image were corrected with respect to the USB light microscope image. See also curved arrows numbered by "1." in Figure 5.
2. Consecutive similarity-based elastic registrations (initialized by landmarks) of confocal images from physical slices lying on the present slide, i.e., the (floating) images of the second physical slice were aligned with respect to the images (now fixed) of the first physical slice, the (floating) images of the third physical slice with respect to the images of the second physical slice (now fixed), etc. See curved arrows numbered by "2., 3., . . . , n(k)+1" in Figure 5.
3. The steps 1–2 were repeated for all microscopic slides.

As mentioned earlier, the thickness of physical slices was 30 μm, and there were six to eight physical slices per one microscopic slide. Thus, one USB light microscope image was used to correct confocal data captured from the specimen of thickness from 180 to 240 μm. Because of the fact that the area of embryo sections (circa 23 mm^2) was much larger than the thickness of the physical slices, and that the USB light microscope images characterized particularly main features of the embryo, the above procedure resulted in correct reconstruction. At the same time, the procedure reduced user's effort, thanks to performing approximately only a half of elastic registrations compared to the case of correcting each physical slice by the corresponding USB light microscope image.

By applying the first procedure, we obtained a set of volumes corresponding to individual microscopic slides, and in the next procedure, we registered that set together to obtain the whole reconstructed volume:

The second procedure (Fig. 5):

1. Similarity-based elastic registration (initialized by landmarks) of the last image (floating) of the reconstructed volume of the present slide with the first image (fixed) of the volume of the next slide. See the bold arrow numbered by Roman numeral "I." in Figure 5.
2. Applying elastic transformation found in the previous step to all images of the volume of the present slide with linear decreasing weights of influence of elastic transformation on images, i.e., the last image of the present volume was transformed with the full weight, the last but one image with a lowered weight, . . . , the first image of the present volume remained intact. See the bold arrow numbered by Roman numeral "II." in Figure 5.
3. The steps 1–2 were repeated for all microscopic slides.

Applying linearly decreased weights of elastic transformation to images yielded a sliding effect of related USB light microscope images on the reconstruction from confocal data. Consecutive use of the procedures lead to the fact that the confocal volume of the i-th slide was elastically corrected partly by the USB light microscope image corresponding to the present slide and partly by the USB light microscope image corresponding to the (i+1)-th slide. The effect of elastic deformations on a present image of the volume of the i-th slide was linearly proportional to the distance of the image from the two USB light microscope images.

Thus, the second procedure ensured smooth reconstruction of the whole volume using data of all microscopic slides, and at the same time it preserved corrections that came from USB light microscope images.

Image Enhancement of Optical Sections

Fluorescent images, captured by a CLSM, suffered from light loss degradations which could be described by two main effects—light aberration and photobleaching (Diaspro, 2002). When different physical slices were captured by the CLSM, it was difficult in practice to maintain the same brightness among images because of variability in fluorescence signal, saturation

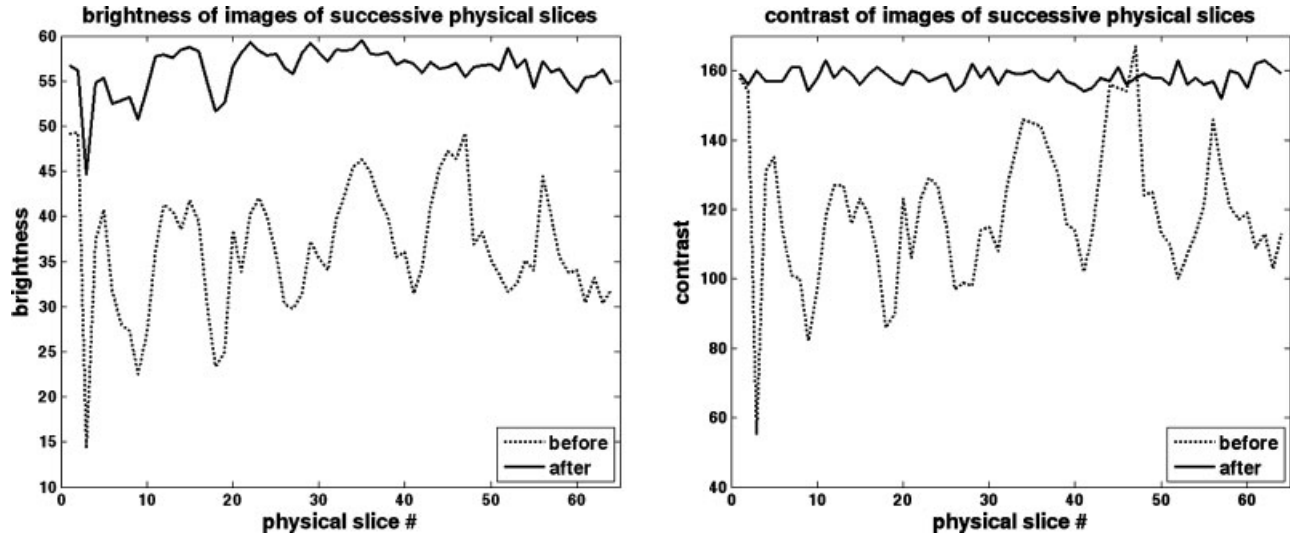

Fig. 6. Brightness (left) and contrast (right) curves of images of physical slices in the resulting high-resolution volume: dotted lines–before brightness or contrast compensation, solid lines–after the compensation.

of tissues by fluorescent dyes, different depth of focus of the laser beam, etc. The light variations were intensified by the fact that the physical slices remained embedded in paraffine to reduce deformations. As a result, images from different physical slices had different brightness and contrast levels, see Figure 6. This could cause problems in subsequent volume reconstruction and following image processing tasks like analysis, measurement, segmentation, and visualization of objects. Therefore, we applied methods for compensation of such a light variability described by Čapek et al. (2006).

Assessment of Deformation Errors

We evaluated deformation errors created by specimen cutting and manipulation with physical slices while placing them on microscopic slides. We compared images captured by the USB light microscope from the cutting planes of the first physical slices of the slides with the corresponding images of these slices captured by CLSM, i.e., 10 pairs of images; see, for example, Figure 4. For this comparison, we used the following two methods: First, we evaluated global shapes of depicted objects by the mean Procrustes shape distance metric (Bookstein, 1997). Second, we measured the area of objects by a stereological point counting method (Kubínová et al., 2006).

The mean Procrustes distance is a least-squares type shape metric that requires shapes with one-to-one point correspondence. Determination of the Procrustes distance between two shapes involves alignment of the shapes with respect to position and orientation. The shapes are given by landmarks manually inserted on corresponding features in both images. After shape alignment, the mean Procrustes distance can be expressed by the formula

$$P_{\mathrm{D}} = \sqrt{\frac{1}{n}\sum_{j=1}^{n}\left[\left(x_{j1}-x_{j2}\right)^2+\left(y_{j1}-y_{j2}\right)^2\right]}, \qquad (2)$$

where x, y are coordinates of landmarks and n represents their number.

To describe errors in individual directions, we also computed differences of landmark positions as absolute valued mean errors of their coordinates:

$$\Delta x = \frac{1}{n}\sum_{j=1}^{n}\left|x_{j1}-x_{j2}\right|, \qquad (3)$$

$$\Delta y = \frac{1}{n}\sum_{j=1}^{n}\left|y_{j1}-y_{j2}\right| \qquad (4)$$

When measuring areas of objects in slices by the stereological point counting method, a grid of uniformly spatially distributed points is virtually superimposed over the slice. The points which are inside the investigated objects are interactively selected by a user, and thus the area of objects is estimated by the number of points multiplied by the area corresponding to one test point. Accuracy of the measurement is given by a priori chosen density of points in the point grid.

RESULTS

The volume reconstruction of the part of a rat embryo was carried out, as described above, and shown in the following figures: Figure 2 exemplifies horizontal stitching (mosaicking) of eight overlapping fields of view into a resulting mosaic image. Mosaicking was performed using the *GlueMRC* software. Figure 3 shows a typical example of elastic registration of confocal images of consecutive physical slices. The result of

TABLE 1. Differences in areas measured by a stereological point counting method (ΔA), Procrustes distance (PD), and mean errors of x and y coordinates (Δx, Δy) of embryos depicted in confocal images and corresponding USB light microscope images.

Glass #	ΔA Orig [μm^2]	ΔA Reg [μm^2]	*PD* Orig [μm]	*PD* Reg [μm]	Δx Orig [μm]	Δx Reg [μm]	Δy Orig [μm]	Δy Reg [μm]
1	2987×10^3	59×10^3	42.4	17.0	28.2	7.6	16.2	9.3
2	-125×10^3	-43×10^3	20.8	19.6	6.6	6.1	12.4	14.8
3	148×10^3	95×10^3	22.8	19.4	8.7	6.8	11.8	9.2
4	434×10^3	-72×10^3	28.7	19.7	16.9	7.7	15.7	13.9
5	243×10^3	-49×10^3	25.5	17.9	16.1	11.7	12.6	9.9
6	530×10^3	148×10^3	29.7	18.3	20.8	9.0	16.6	9.8
7	454×10^3	388×10^3	32.5	28.2	18.6	18.1	18.8	18.6
8	-355×10^3	134×10^3	37.9	24.0	15.2	10.7	28.4	16.8
9	174×10^3	-141×10^3	28.2	20.2	8.2	10.3	21.5	14.6
10	382×10^3	269×10^3	19.0	14.1	8.9	6.9	13.6	8.3
ø	487×10^3	79×10^3	28.8	19.8	20.4	8.5	16.8	12.5
σ^2	762×10^3	24×10^3	49.0	13.1	73.0	12.3	23.5	12.0

All values are both before (Orig) and after registration (Reg). The last two rows of the table show mean values (ø) and variances (σ^2) of corresponding columns, respectively. The area of embryo sections was approximately 23 mm^2.

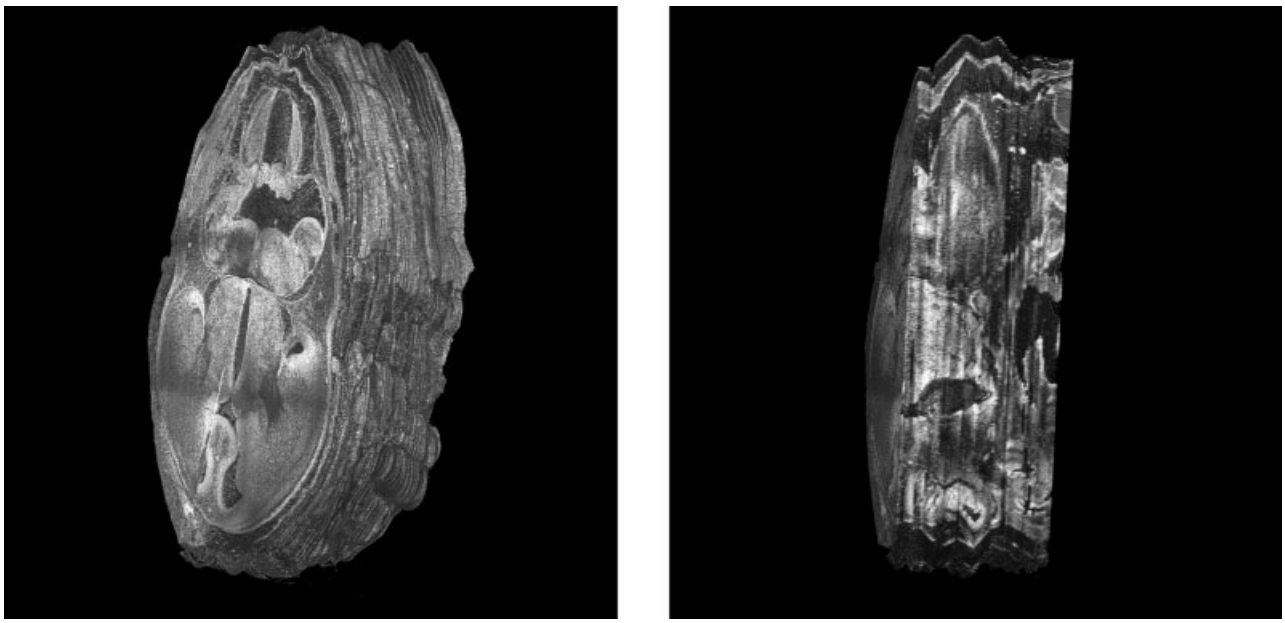

Fig. 7. Volume rendering of the resulting high-resolution volume of the part of a rat embryo: the left image–the whole volume, the right one–a virtual cut through the volume using a virtual plane. Note that internal structures of the embryo are well matched.

registration can be seen in Figure 3b whereas 3c shows the elastic deformation mask applied.

Further, we evaluated deformation errors between corresponding USB light microscope images and confocal images. The results are shown in Table 1. We can see that all values of registered images show improvement in object alignment after performing registration, which resulted in improvement of volume reconstruction. Especially, in case of the first slide, we can observe huge deformation of the confocal image with respect to its corresponding USB light microscope image, but the deformation was repaired by the registration of the images.

From the Table, it follows that in all cases the elastic registration algorithm matched the embryo well. However, because of limitation of elastic registration algorithms, especially the requirement of optimization of high number of parameters, which is generally a difficult and computationally ambiguous task, small areas remained partially deformed causing errors in area differences measured, e.g., by the stereological method. Moreover, sometimes it was difficult to find the exact location of corresponding features in both types of images because of applying different modalities (confocal fluorescence microscope versus USB light microscope) for acquisition. The stereological method itself has a measurement error.

Figure 6 demonstrates the effect of the light variability (brightness and contrast) of images of successive physical slices. The image contrast, depicted in Figure 6-right, was computed (denoted by C_i for the i-th image) as a difference between intensity values corresponding to the 90th percentile $p_{90,i}$ and the 10th percentile $p_{10,i}$ of the image histogram:

$$C_i = p_{90,i} - p_{10,i}. \quad (5)$$

Finally, Figure 7 shows examples of 3D volume rendering visualizations of the reconstructed high-resolution volume of the part of a rat embryo. The resulting gray-

scale volume consists of 1166 × 1744 × 256 voxels. Volume rendering was performed using a *VolumePro 1000* hardware board (Pfister et al., 1999).

DISCUSSION

Requirements for successful volume reconstruction using our approach are as follows: (A) Careful preparation of the tissue specimen to decrease the off-cut and the extent of spatial deformations along the z-axis for successful registration of successive physical slices. (B) Sufficient overlap of neighboring horizontal fields of view sharing the same parts of depicted objects/structures for proper mosaicking. (C) Reasonably, well depicted objects or structures in stacks of optical sections with a satisfactory signal-to-noise ratio.

For successful volume reconstruction, it is also necessary to choose an appropriate objective and the size of image pixels, i.e., the resolution of acquired images of optical sections. When high level of details is required, a high magnification objective and high resolution of images must be chosen. However, this increases the amount of captured image data, because more horizontal fields of view and more optical sections within one stack are required to cover a physical slice than with a low magnification objective. Therefore, a compromise must be found. In this work, we demonstrated the volume reconstruction on a 3D visualization of a rat embryo. Because physical slices of this object were large, we used a low magnification (5×) objective with a low numerical aperture (NA = 0.15). The optimum distance in z-direction, inversely proportional to the square of the NA as explained by Diaspro (2002), found by the CLSM software, was about 10 μm between subsequent optical sections.

We solved the problem of propagation of deformations through the resulting reconstructed volume by elastic registration. For this purpose, we utilized a priori information about the embryo captured by the USB light microscope from cutting planes of the paraffine block during histological sectioning. We captured one USB light microscope image per a set of physical slices carried by a single microscopic slide and performed registration of these images with corresponding confocal images. We further evaluated the deformation errors using a stereological measurement and the Procrustes distance, and found that applying the registration decreases the extent of these deformations in the resulting reconstruction.

Both mosaicking and vertical linking of data sets are based on registration via optimizing a similarity measure between images to be aligned. In most cases, this is a convenient approach, because biological confocal data contain acceptable depicted objects or structures that can be aligned with respect to each other. Another approach, commonly used in microscopy, is registering images utilizing external artificial markers or internal salient features (found or segmented in captured images), as described, e.g., by Bajcsy et al. (2006). In our case, external markers are difficult to create because these would have to be inserted into a tissue several millimeters thick, which would result in undesirable additional deformations.

Mosaicking of neighboring overlapping fields of view is performed using the *GlueMRC* software (Karen et al., 2003), which is presently not included in the *Rapid3D* system. Mosaicking can be enhanced by using a motorized microscopic stage, allowing automatically capturing neighboring fields of view, which is in preparation.

Volume reconstruction of biological tissues is a laborious and time demanding process, especially if there is a large number of horizontal fields of view required to cover one physical slice, and if many physical slices must be cut from the tissue specimen. There are other techniques than those based on registration of images from serial physical sections. These are, for instance, two-photon tissue cytometry (Kim et al., 2007), selective plane illumination microscopy (Huisken et al., 2004), and optical computed or emission tomography (Oldham et al., 2007). The advantage of such techniques lies in the possibility to capture large specimens with high contrast and high resolution without the necessity of image alignment. However, these are dedicated systems and at the moment of writing this article not publicly available.

In contrast, our approach exploits a standard confocal microscope for reconstruction, and even low-cost CLSM systems are sufficient for this task. Moreover, the size of the investigated specimen can be large (up to centimeters) with resolution of resulting 3D images depending on the resolution of stacks of images of optical sections.

To summarize, primary intention of this work was to develop a framework covering methods for 3D reconstruction and visualization of large biomedical tissues from confocal image data. We implemented corresponding software package, called *Rapid3D*, helping biologists and technicians to achieve this goal. To our knowledge, such complex software system is not available elsewhere yet.

Rapid3D is a user-friendly software package offering algorithms for efficient volume reconstruction of tissues captured by CLSM. The package includes reading/writing of image data, elastic registration and linking of mosaic images of successive physical slices, enhancement of images in the resulting high-resolution volume, restoration of true shapes and sizes of objects after elastic registration using a priori information, and 2D and 3D visualization of image data sets. Interactive volume visualization is accomplished both by using a VolumePro 1000 hardware rendering board (TeraRecon, USA), and by employing OpenGL and DirectX technologies supported by common graphics cards. Thus, *Rapid3D* represents a useful tool for 3D reconstruction and visualization of large tissue volumes with sufficient resolution for a number of biological studies in histology, embryology, evolution biology, and developmental biology.

ACKNOWLEDGMENTS

We thank Lucie Kocandová (Institute of Physiology ASCR, Prague) for her help with acquisition of confocal images and with stereological measurements, Dr. Jan Michálek (Institute of Physiology ASCR, Prague), and Dr. Marie Jirkovská (Institute of Histology and Embryology, 1st Faculty of Medicine, Charles University, Prague, Czech Republic) for their helpful comments.

REFERENCES

Bajcsy P, Lee SC, Lin A, Folberg R. 2006. Three-dimensional volume reconstruction of extracellular matrix proteins in uveal melanoma from fluorescent confocal laser scanning microscope images. J Microsc 221:30–45.

Bookstein FL. 1997. Landmark methods for forms without landmarks: Morphometrics of group differences in outline shape. Med Image Anal 1:225–243.

Čapek M, Krekule I. 1999. Alignment of adjacent picture frames captured by a CLSM. IEEE Trans Inf Technol Biomed 3:119–124.

Čapek M, Janáček J, Kubínová L. 2006. Methods for compensation of the light attenuation with depth of images captured by a confocal microscope. Microsc Res Tech 69:624–635.

Cerri PS, de Faria FP, Villa RG, Katchburian E. 2004. Light microscopy and computer three-dimensional reconstruction of the blood capillaries of the enamel organ of rat molar tooth germs. J Anat 204:91–195.

Cornillie P, Van Den Broeck W, Simoens P. 2008. Three-dimensional reconstruction of the remodeling of the systemic vasculature in early pig embryos. Microsc Res Tech 71:105–111.

Diaspro A, editor. 2002. Confocal and two-photon microscopy, foundation, applications, and advances. New York: Wiley.

Diaspro A, Bianchini P, Vicidomini G, Faretta M, Ramoino P, Usai C. 2006. Multi-photon excitation microscopy. BioMed Eng OnLine 5:36. Doi:10.1186/1475-925X-5-36. Available online.

Difato F, Mazzone F, Scaglione S, Fato M, Beltrame F, Kubínová L, Janáček J, Ramoino P, Vicidomini G, Diaspro A. 2004. Improvement in volume estimation from confocal sections after image deconvolution. Microsc Res Tech 64:151–155.

Duerstock BS. 2004. Double labeling serial sections to enhance three-dimensional imaging of injured spinal cord. J Neurosci Methods 134:101–107.

Duerstock BS, Bajaj CL, Borgens RB. 2003. A comparative study of the quantitative accuracy of three-dimensional reconstructions of spinal cord from serial histological sections. J Microsc 210:138–148.

Fernandez-Gonzalez R, Jones A, Garcia-Rodriguez E, Chen PY, Idica A, Lockett SJ, Barcellos-Hoff MH, Ortiz-De-Solorzano C. 2002. System for combined three-dimensional morphological and molecular analysis of thick tissue specimens Microsc Res Tech 59:522–530.

Huisken J, Swoger J, Del Bene F, Wittbrodt J, Stelzer EHK. 2004. Optical sectioning deep inside live embryos by selective plane illumination microscopy. Science 305:1007–1009.

Jirkovská M, Kubínová L, Janáček J, Moravcová M, Krejčí V, Karen P. 2002. Topological properties and spatial organization of villous capillaries in normal and diabetic placentas. J Vasc Res 39:268–278.

Jirkovská M, Náprstková I, Janáček J, Kučera T, Macášek J, Karen P, Kubínová L. 2005. Three-dimensional reconstructions from non-deparaffinized tissue sections. Anat Embryol 210:163–173.

Karen P, Jirkovská M, Tomori Z, Demjénová E, Janáček J, Kubínová L. 2003. Three-dimensional computer reconstruction of large tissue volumes based on composing series of high-resolution confocal images by GlueMRC and LinkMRC software. Microsc Res Tech 62:415–422.

Kim KH, Ragan T, Previte MJR, Bahlmann K, Harley BA, Wiktor-Brown DM, Stitt MS, Hendricks CA, Almeida KH, Engelward BP, So PTC. 2007. Three-dimensional tissue cytometer based on high-speed multiphoton microscopy. Cytometry A 71A:991–100.

Kubínová L, Janáček J, Krekule I. 2006. Stereological methods for estimating geometrical parameters of microscopic structure by three-dimensional imaging. In: Diaspro A, editor. Confocal and two-photon microscopy, foundation, applications, and advances. New York: Wiley, pp. 299–332.

Kurien T, Boyce RWG, Paish EC, Ronan J, Maddison J, Rakha EA, Green AR, Ellis IO. 2005. Three dimensional reconstruction of a human breast carcinoma using routine laboratory equipment and immunohistochemistry. J Clin Pathol 58:968–972.

Lee KJ, Park ChH, Rhyu IJ. 2005. Efficient three-dimensional reconstruction of synapse with high-voltage electron microscopy. J Electron Microsc (Tokyo) 54:139–141.

Lee SC, Bajcsy P. 2005. Feature based registration of fluorescent LSCM imagery using region centroids. Proc SPIE 5747-128:170–181.

Lee SC, Bajcsy P. 2007. Trajectory fusion for three-dimensional volume reconstruction. Comput Vis Image Understand. Doi:10.1016/j.cviu. 2007.02.005. Available online.

Liu S, Weaver DL, Taatjes DJ. 1997. Three-dimensional reconstruction by confocal laser scanning microscopy in routine pathologic specimens of benign and malignant lesions of the human breast. Histochem Cell Biol 107:267–278.

Oldham M, Sakhalkar H, Wang YM, Guo P, Oliver T, Bentley R, Vujaskovic Z, Dewhirst M. 2007. Three-dimensional imaging of whole rodent organs using optical computed and emission tomography. J Biomed Opt 12:014009.

Ovtscharoff W, Segal M, Goldin M, Helmeke C, Kreher U, Greenberger V, Herzog A, Michaelis B, Braun K. 2008. Electron microscopic 3D-reconstruction of dendritic spines in cultured hippocampal neurons undergoing synaptic plasticity. 68:870–876.

Pawley JB, editor. 2006. Handbook of biological confocal microscopy. 3rd ed. Berlin: Springer.

Papadimitriou C, Yapijakis C, Davaki P. 2004. Use of truncated pyramid representation methodology in three-dimensional reconstruction: an example. J Microsc 214:70–75.

Pfister H, Hardenbergh J, Knittel J, Lauer H, Seiler L. 1999. The VolumePro real-time ray-casting system. 1999 Proc. SIGGRAPH Conf:251–260.

Sorzano COS, Thévenaz P, Unser M. 2005. Elastic registration of biological, images using vector-spline regularization. IEEE Trans Biomed Eng 52:652–663.

Tekalp AM. 1995. Digital video processing. New York: Prentice Hall.

Zitová B, Flusser J. 2003. Image registration methods: A survey. Image Vis Comp 21:977–1000.